JOURNAL OF MATERIALS SCIENCE 28 (1993) 2289–2298

Role of hydrostatic stress in hydrogen diffusion in pearlitic steel

J. TORIBIO
Department of Materials Science, Polytechnical University of Madrid, E.T.S.I. Caminos, Ciudad Universitaria, 28040 Madrid, Spain

The relevant role of hydrostatic stress in hydrogen diffusion in pearlitic steel is outlined from both theoretical and experimental points of view. The theoretical development offers the formulation of hydrogen diffusion equations where hydrogen flux density depends not only on the concentration gradient, but also on the hydrostatic stress distribution in the sample. The experimental programme consisted of slow strain-rate tests on axisymmetric notched samples at different strain rates under simultaneous hydrogen charging by cathodic polarization. The use of different notch geometries allows a study of the influence on hydrogen diffusion of the hydrostatic stress state in the vicinity of the notch tip. A specific microscopic mode of fracture different from classical cleavage was found, associated with hydrogen effects: the tearing topography surface. In the quasi-instantaneous tests, the value of hydrostatic stress at the sample boundary (just the notch tip) at the failure instant is relevant from the fracture point of view. In the quasi-static tests, the tearing topography surface depth equals that of the maximum hydrostatic stress point, and the maximum value of the stress triaxiality in each geometry (ratio of the hydrostatic to the equivalent stress, almost constant during the tests) seems to govern the diffusion process. These facts emphasize the relevant role of hydrostatic stress in the vicinity of the notch in hydrogen diffusion.

1. Introduction

Hydrogen embrittlement, with loss of ductility and decrease of fracture resistance, plays an important role in environmentally assisted cracking, that is, in all fracture processes of metals subjected to aggressive environments. When a sample is tested in a corrosive medium with electrochemical techniques, hydrogen embrittlement is a phenomenon associated not only with cathodic potentials, but also with anodic ones, although in the latter case the main damage mechanism is anodic dissolution [1]. The hydrogen transport phenomena in iron and steel have been studied by many researchers, but the results are sometimes contradictory, and the problem is not yet fully understood [2].

Two main types of hydrogen transport in metals have been proposed. The first is random walk or lattice diffusion [3–7], in which hydrogen diffuses through the crystalline lattice of the metal. The mathematical approach to this phenomenon is by way of Fick's laws, which can be modified to take account of physical variables such as temperature, density of hydrogen traps, sulphur content, etc. In addition, the theoretical bases of Fick's laws may be improved, introducing the dependence of hydrogen flux on the hydrostatic stress field in the sample, an assumption based on physical reasons. This stress-assisted diffusion provides penetration distances deeper than those calculated from the classical Fick's diffusion. Models of hydrogen embrittlement in accordance with this approach have appeared in previous works [8, 9].

The other mechanism of hydrogen transport is dislocation sweeping [10, 11]. Two kinetic models were proposed for predicting the hydrogen local enrichment: the stripping model by Tien *et al.* [12], and the annihilation model by Johnson and Hirth [13], both recently reviewed [14], predicting a significant enrichment of hydrogen at internal trap boundaries. Some researchers, however, do not consider dislocation transport as a critical step for hydrogen embrittlement [15, 16], or do not observe accelerating effects of plastic deformation on hydrogen transport [17].

The possibility of a mixed hydrogen transport mechanism including both lattice diffusion and dislocation dragging should be considered. The predominance of one or another may depend on the experimental conditions [18]. Even considering only dislocation sweeping, the adsorption of hydrogen near dislocations and cracks is governed by stress-assisted diffusion equations [19, 20]. From the computational point of view, it is possible to find approaches which include dislocation transport in the hydrogen-diffusion equations, by considering an effective diffusion coefficient dependent on dislocation density, which is a function of equivalent plastic strain [21, 22].

Consideration should be given to hydrogen trapping, which has been known for many years [23, 24], and affects diffusivity profoundly, with less effect on dislocation transport of hydrogen. The trapping characteristics of the metal depend on its microstructure [25], it being possible to distinguish between reversible and irreversible traps [26]. Models of hydrogen

0022–2461

trapping including both kinds of trap have been formulated in the past [27–32]. In high-strength alloys the most plausible traps appear to be MnS inclusions [33].

The aim of the present work was to formulate, on the basis of thermodynamic considerations, equations for stress-assisted diffusion of hydrogen in metals, including not only the effect of the concentration differences, but also that of the hydrostatic stress gradient, which conditions the transport, making the hydrogen diffuse towards the regions of maximum hydrostatic stress and modifying the boundary condition for the diffusion partial differential equation. Consequently, the role of hydrostatic stress in hydrogen embrittlement phenomena is outlined.

2. Diffusion equations

A thermodynamic formulation of the diffusion problem, based on the Gibbs free enthalpy, is proposed in this section. In the case of small strains and low hydrogen concentrations the linear theory represents a first approach, and the Gibbs function for the thermodynamic system hydrogen–metal takes the form [34]

$$G = -\frac{\alpha}{2}(\mathrm{tr}\,\boldsymbol{\sigma})^2 - \frac{\beta}{2}\boldsymbol{\sigma}\cdot\boldsymbol{\sigma} - \gamma c\,\mathrm{tr}\,\boldsymbol{\sigma} + f(c) \quad (1)$$

where α, β and γ are constants, c represents the hydrogen concentration and $\boldsymbol{\sigma}$ is the stress tensor; $\boldsymbol{\sigma}\cdot\boldsymbol{\sigma}$ is the inner product (or scalar product) of the tensors (the expression in components is $\boldsymbol{\sigma}\cdot\boldsymbol{\sigma} = \sigma_{ij}\sigma_{ij}$), $f(c)$ represents any function of the concentration. Assuming that $f(c)$ takes the form of an integral of a logarithm, a modified formulation for the classical Fick's laws of diffusion can be obtained. The expression for G is then

$$G = -\frac{\alpha}{2}(\mathrm{tr}\,\boldsymbol{\sigma})^2 - \frac{\beta}{2}\boldsymbol{\sigma}\cdot\boldsymbol{\sigma} - \gamma c\,\mathrm{tr}\,\boldsymbol{\sigma} + k\int \ln c\,\mathrm{d}c \quad (2)$$

in which k is a new constant.

The chemical potential of hydrogen can be obtained by deriving the Gibbs function

$$\mu_H = \frac{\partial G}{\partial c} = k\ln c - \gamma\,\mathrm{tr}\,\boldsymbol{\sigma} \quad (3)$$

The relative velocity between the hydrogen and the metal proceeds from the chemical potential

$$v = -m\,\mathbf{grad}\,\mu_H \quad (4)$$

where m is a constant and v the relative velocity. From this equation, the hydrogen flux density $\boldsymbol{J}$ is

$$\boldsymbol{J} = -mc\,\mathbf{grad}\,\mu_H \quad (5)$$

By substituting the expression of μ_H given in Equation 3, a modification of Fick's First Law is obtained, which takes into account the effect of the stress field in the metal on the hydrogen flux density:

$$\boldsymbol{J} = -km\,\mathbf{grad}\,c + \gamma mc\,\mathbf{grad}\,(\mathrm{tr}\,\boldsymbol{\sigma}) \quad (6)$$

where the term dependent on the stress tensor trace and thus on the hydrostatic stress, σ, is significant

$$\sigma = \mathrm{tr}\,\boldsymbol{\sigma}/3 \quad (7)$$

Applying the conservation of mass to a volume, V, limited by a surface, S, invariable with time, gives

$$\frac{\partial}{\partial t}\int_V c\,\mathrm{d}V = -\int_S \boldsymbol{J}\cdot\mathrm{d}S \quad (8)$$

Following Gauss's theorem, the continuity equation is obtained

$$\frac{\partial c}{\partial t} = -\mathrm{div}\,\boldsymbol{J} \quad (9)$$

Substituting the expression of $\boldsymbol{J}$ given in Equation 6, a partial differential equation is obtained, which is a modification of Fick's Second Law

$$\frac{\partial c}{\partial t} = km\Delta c - \gamma m\,\mathbf{grad}\,c\cdot\mathbf{grad}\,(\mathrm{tr}\,\boldsymbol{\sigma}) - \gamma mc\Delta(\mathrm{tr}\,\boldsymbol{\sigma}) \quad (10)$$

where Δ is the Laplacian operator, defined as the divergence of the gradient: $\Delta u = \mathrm{div}\,(\mathbf{grad}\,u)$.

If the material is linear and elastic, the latter term $\Delta(\mathrm{tr}\,\boldsymbol{\sigma})$ becomes zero, from the constitutive and compatibility equations

$$\boldsymbol{\sigma} = \lambda(\mathrm{tr}\,\boldsymbol{\epsilon})\mathbf{1} + 2\mu\boldsymbol{\epsilon} \quad (11)$$

$$\boldsymbol{\epsilon} = (\mathbf{grad}\,u + \mathbf{grad}^{\mathrm{T}}\boldsymbol{u})/2 \quad (12)$$

where $\boldsymbol{\epsilon}$ is the strain tensor, $\mathbf{1}$ the unity tensor, $\boldsymbol{u}$ the displacement vector, and λ and μ the Lamé coefficients.

The most common boundary condition for the differential Equation 10 is that of free metal boundary in contact with the hydrogen, and this is given in terms of a chemical potential

$$\mu_H = \mu_H^0 \quad (13)$$

or, in other terms

$$k\ln c - \gamma\,\mathrm{tr}\,\boldsymbol{\sigma} = k\ln c_0 \quad (14)$$

where c_0 is the concentration for hydrogen–metal equilibrium, when the latter is free of stress. Thus

$$c = c_0\exp\left(\frac{\gamma}{k}\,\mathrm{tr}\,\boldsymbol{\sigma}\right) \quad (15)$$

an equation which represents both the boundary condition for the diffusion problem and the stationary solution of the problem.

The elastic strains in the metal can be calculated through derivation of the Gibbs function (Equation 2)

$$\boldsymbol{\epsilon}^{\mathrm{e}} = -\frac{\partial G}{\partial \boldsymbol{\sigma}} = \alpha(\mathrm{tr}\,\boldsymbol{\sigma})\mathbf{1} + \beta\boldsymbol{\sigma} + \gamma c\mathbf{1} \quad (16)$$

and the increment of the strain tensor due only to the hydrogen is

$$(\Delta^*\boldsymbol{\epsilon}^{\mathrm{e}})_{\mathrm{c}} = \gamma(\Delta^* c)\mathbf{1} \quad (17)$$

where Δ^* represents the increment, to distinguish it from Δ (Laplacian operator).

Equation 15 can be expanded in Taylor's series

$$c = c_0\left[1 + \frac{\gamma}{k}\mathrm{tr}\,\boldsymbol{\sigma} + \frac{1}{2}\left(\frac{\gamma}{k}\mathrm{tr}\,\boldsymbol{\sigma}\right)^2 + \ldots\right] \quad (18)$$

and considering only the first two terms

$$\Delta^* c = \frac{\gamma}{k} c_0 \Delta^*(\mathrm{tr}\,\boldsymbol{\sigma}) \quad (19)$$

and substituting in Equation 17, this yields

$$(\Delta^* \boldsymbol{\epsilon}^e)_c = \frac{\gamma^2}{k} c_0 \Delta^*(\mathrm{tr}\,\boldsymbol{\sigma})\,\mathbf{1} \quad (20)$$

the increment of elastic strain due to the hydrogen, a term which modifies the constitutive equation of the metal. This term is negligible on assuming that ingress of hydrogen into the steel is achieved by means of a non-pressurized atmosphere, as in the case of cathodic polarization, where hydrogen naturally enters by differences in concentration or hydrostatic stress from one point to another. In this case the stress–strain relationship is the one corresponding to an inert environment.

Modified Fick's laws (Equations 6 and 10) can be written with the usual symbols

$$\boldsymbol{J} = -D^* \mathbf{grad}\, c + Mc\,\mathbf{grad}\,\sigma \quad (21)$$

$$\frac{\partial c}{\partial t} = D^* \Delta c - M\,\mathbf{grad}\, c \cdot \mathbf{grad}\,\sigma - Mc\Delta\sigma \quad (22)$$

where σ is the hydrostatic stress ($\sigma = \mathrm{tr}\,\boldsymbol{\sigma}/3$), D^* the hydrogen diffusion coefficient and M a second coefficient, a function of the first

$$M = \frac{D^* V^*}{RT} \quad (23)$$

in which V^* is the molar partial volume of hydrogen, R the ideal gases constant and T the absolute temperature.

The relationships between the constants k, γ and m used in the present formulation and the common diffusion coefficients are the following

$$km = D^* \quad (24a)$$

$$3\gamma m = M \quad (24b)$$

$$3\gamma/k = V^*/RT \quad (24c)$$

The boundary condition (Equation 15) yields

$$c = c_0 \exp\left(\frac{V^*\sigma}{RT}\right) \quad (25)$$

Boltzmann's distribution, where c_0 is the equilibrium concentration without stress. This equation is also the stationary solution of the diffusion problem.

In the quasi-instantaneous tests (fast enough to assume that there is no hydrogen diffusion towards the inner points), the hydrogen concentration at the boundary is a direct function of the hydrostatic stress at that point

$$c_\Gamma = c_0 \exp\left(\frac{V^*\sigma_\Gamma}{RT}\right) \quad (26)$$

In the quasi-static tests (slow enough to neglect time effects) the situation approaches the stationary one, and the concentration at all points on the sample is a direct function of the hydrostatic stress at those points

$$c(x) = c_0 \exp\left(\frac{V^*\sigma(x)}{RT}\right) \quad (27)$$

3. Experimental details

3.1. Procedure

To analyse the role of hydrostatic stress in hydrogen diffusion in pearlitic steel, slow strain-rate tests (SSRT) were performed on round-notched samples in an aqueous medium which promoted hydrogen embrittlement. Different notch geometries (a wide range of notch depths and radii) were used to achieve different hydrostatic stress distributions in the vicinity of the notch and so influence the hydrogen diffusion according to the equations developed in the previous section. In the SSRT the sample is subjected to an externally applied constant displacement rate up to fracture. This method presents some advantages when compared to constant load or constant strain tests, the main one being the measurement of a more significant physical parameter as the critical load or strain at the fracture instant, not only the critical time measured in constant load or constant strain tests. Furthermore, the use of notched specimens favours the localization of the environmental attack just at the crack or notch tip, thus decreasing experimental scatter.

The material used in this investigation was a hot-rolled pearlitic steel supplied from commercial stock by Nueva Montaña Quijano Company (Santander, Spain), in bar form of 12 mm diameter. This steel presents a coarse pearlitic microstructure (austenite grain size 75 μm, pearlite interlamellar spacing 0.3 μm). It is the steel used in the production of cold-drawn wire for prestressed concrete, after patenting in a molten lead bath to produce fine pearlite (interlamellar spacing around 0.1 μm). Chemical composition and mechanical properties are given in Tables I and II respectively.

Tests were performed on round-notched samples with the four notch geometries sketched in Fig. 1. The dimensions of the samples were as given in Table III, where R is the notch radius, A the notch depth and D the diameter of the sample, the latter being $D = 11.25$ mm for all samples tested after machining the supplied 12 mm bars.

The test environment was an aqueous solution of 1 $g\,l^{-1}$ calcium hydroxide plus 0.1 $g\,l^{-1}$ sodium chloride. The pH value was 12.5 and the testing was performed at room temperature (around 17 °C). To promote hydrogen embrittlement, all tests were performed with potentiostatic control at constant potential of − 1200 mV SCE with respect to the saturated calomel electrode (reference). The experimental device appears in Fig. 2, and consists of a potentiostat and

TABLE I Chemical composition

C (%)	Mn (%)	Si (%)	P (%)	S (%)	Fe (%)
0.85	0.60	0.26	< 0.01	< 0.03	Bal.

TABLE II Mechanical properties

Young's modulus (GPa)	Yield strength (MPa)	UTS (MPa)	Elongation under UTS (%)	Ramberg–Osgood parameters $\varepsilon = \sigma/E + (\sigma/P)^n$	
				P (MPa)	n
199	600	1151	6.1	2100	4.9

TABLE III The four notch geometries

Sample	R/D	A/D
A	0.03	0.10
B	0.05	0.39
C	0.36	0.10
D	0.40	0.39

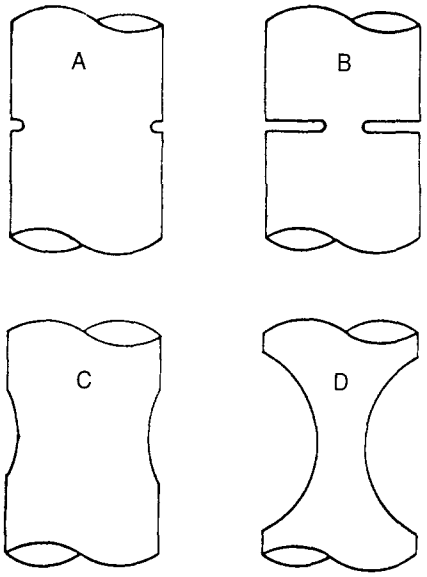

Figure 1 Geometries of the samples (geometry A: $R/D = 0.03$, $A/D = 0.10$; geometry B: $R/D = 0.05$, $A/D = 0.39$; geometry C: $R/D = 0.36$, $A/D = 0.10$; geometry D: $R/D = 0.40$, $A/D = 0.39$, where R is the notch radius, A the notch depth and D the sample diameter).

a classical three-electrode assembly: metallic sample, saturated calomel electrode (reference electrode) and platinum wire (counter electrode).

A broad range of remote displacement rates was covered in the SSRT to evaluate different degrees of hydrogen damage on the samples. Two limit situations are particularly interesting: the quasi-static test, slow enough to reach stationary conditions for the hydrogen diffusion, and the quasi-instantaneous test, fast enough to avoid hydrogen penetration into the sample.

Two fracture tests were performed in air for each geometry, to measure the reference value for the fracture load in the absence of environmental attack. The strain rate externally applied during the tests in air is not a relevant variable in the range of values used in this research, because there is no penetration of external hydrogen in this case.

3.2. Macroscopic results

Macroscopic test results are shown in Fig. 3 for all

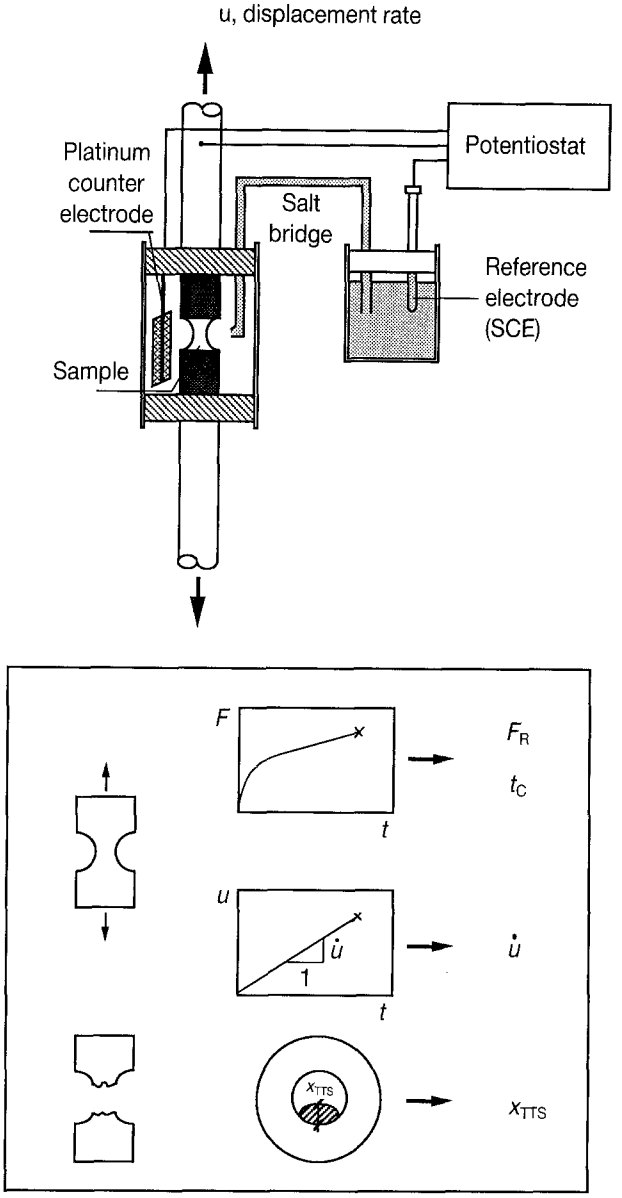

Figure 2 Experimental device for the slow strain-rate tests (SSRT).

geometries, where rupture load in aggressive environment, F_R (normalized to rupture load in air F_0), is plotted versus displacement rate, $\dot{u}$, the former being a monotonic increasing function of the latter. Such results show the well-known trend of hydrogen embrittlement tests when plotted against remote strain rate, either measuring the loss of ductility through the fracture load in the hydrogen atmosphere [35–37], or by means of the reduction in area [38–40]. Both fracture load in hydrogen environment and reduction in area increase as the applied strain rate increases, which would suggest a behaviour influenced by hydrogen diffusion.

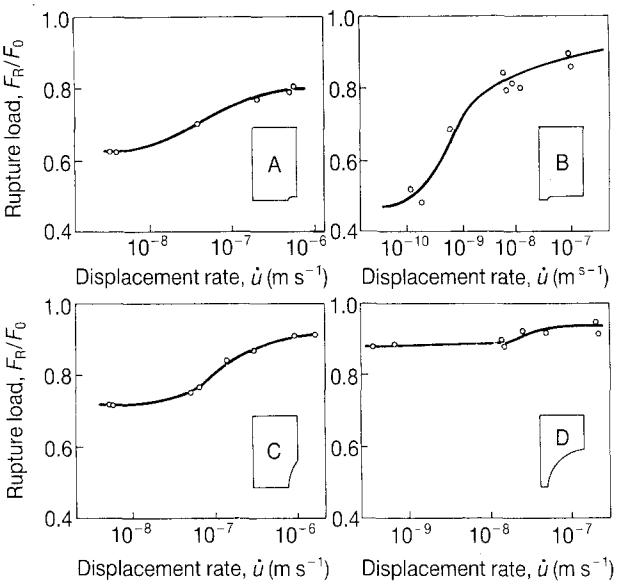

Figure 3 Tests results: rupture load in hydrogen environment (divided by rupture load in air) versus displacement rate.

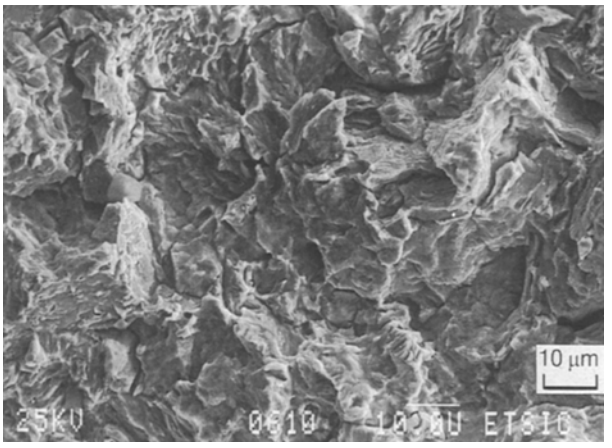

Figure 4 Scanning electron micrograph of the hydrogen-affected area: tearing topography surface (TTS).

For very low values of the strain rate (quasi-static tests), the failure load reaches an asymptotic value corresponding to maximum embrittlement. When the strain rate is below this value, the damage produced by the hydrogen embrittlement does not depend on the strain rate, but on the stress state in the vicinity of the notch tip, and therefore on the geometry. For very high values of the strain rate (ultra-fast tests), the failure load also reaches a limit value corresponding to minimum embrittlement. It is important to emphasize that this value differs from that of the test in air, which indicates that even in a very fast test, the damage produced by the hydrogen embrittlement is not negligible. The consequence is that the internal absorption of the hydrogen adsorbed at the notch surface is practically instantaneous.

3.3. Fractographic analysis

Apart from macroscopic analysis of the rupture of notched samples in a hydrogen atmosphere, it is useful to study the micromechanisms of fracture. Previous research on that topic in pearlitic steel can be found in the literature [41–43] which deals with the role of prior austenite grain size, and [44–47], devoted to the effect of pearlite interlamellar spacing. Other papers [48, 49] analyse the effect of several microstructural variables. Fontaine and Jeunehomme [50, 51] apply the so-called local approach of the fracture to a pearlitic steel. Specific work on hydrogen effects on cleavage fracture of pearlitic steel was performed by Lewandowski and Thompson [52].

Fractographic analysis of the samples used in the present investigation by scanning electron microscopy showed that fracture always initiates at an edge region at the notch tip where the fracture surface may be classified as tearing topography surface (TTS), according to Thompson and co-workers [53, 54]. Fig. 4 is a scanning electron micrograph of such a fracture surface, which looks like a micro-damaged region inside the hydrogen-affected zone. The scale of the microdamage is probably below 1 µm, clearly lower than the prior austenite grain size of the material. Outside the TTS region, fracture surfaces may be classified as cleavage, and clear river patterns can be observed, starting from the TTS region where fracture initiates.

Fig. 5 shows the microscopic fracture modes for all samples. In geometries A and C, the TTS region is always semi-elliptical and is located next to the sample surface, and can be distinguished by simple visual inspection. Geometries B and D, on the other hand, present a ring-shaped TTS region just on the external boundary of the net section, so small that it can be observed only with scanning electron microscope. However, for very low strain rates, (very long times to rupture), the TTS zone for geometries B and D are also of semi-elliptical shape, appreciable by visual inspection. Fig. 2 shows, apart from the experimental device, the procedure for measuring the depth of the TTS region (x_{TTS}) with respect to the notch tip.

4. Discussion

4.1. Interpretation of the tearing topography surface

In discussing the role of diffusion in the hydrogen transport in pearlitic steel, the first key point to be considered is the interpretation of the TTS microscopic fracture mode. The results presented above strongly suggest that the tearing topography surface is associated with hydrogen micro-damage, whereas classical cleavage topography corresponds to unstable fracture.

TTS fracture is not only due to hydrogen alone, but also requires stress (or strain effects), and the rupture takes place when a combination of hydrogen and stress (and also strain) levels is reached, as described in previous papers on fracture of pearlitic steel, (e.g. [43–46, 52]. Nevertheless, there is strong evidence of the afore-mentioned association between TTS mode and hydrogen presence. The first indication is the microscopic mode of fracture attained in the steel under study when fractured in an air environment using exactly the same geometries. In this case, the

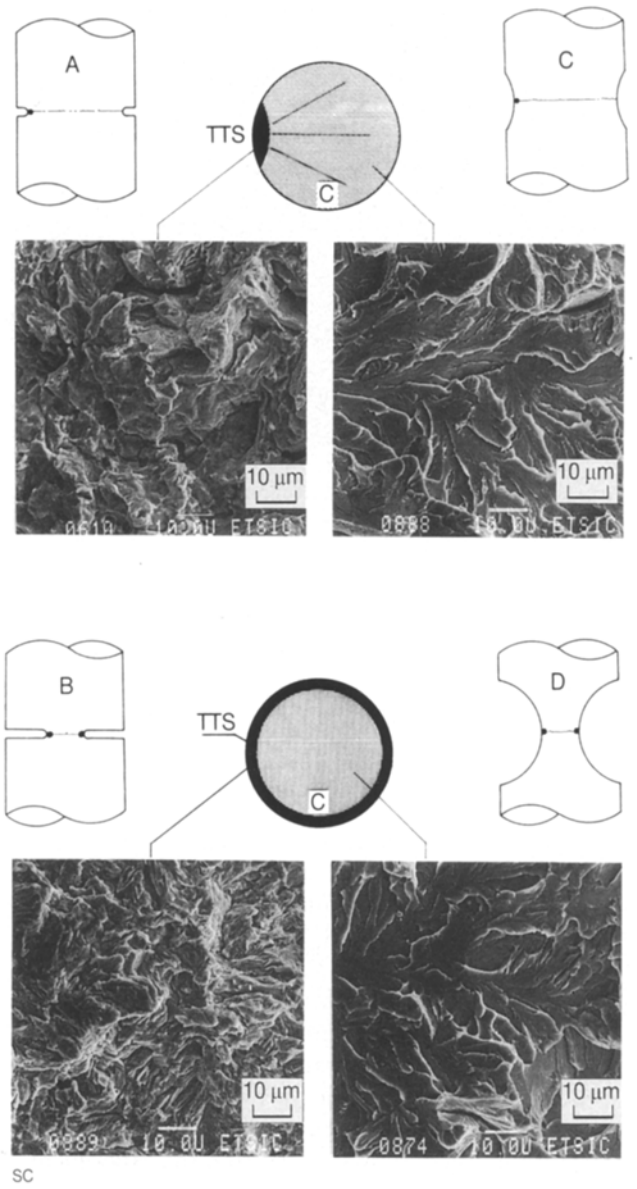

Figure 5 Microscopic fracture modes for all samples (TTS = tearing topography surface; C = cleavage-like).

fracture mode is MVC for the geometry D, and cleavage (initiated by MVC) for geometries A, B and C, as reported by Toribio *et al.* [55]. TTS appears only in the hydrogen atmosphere tests, thereby providing fractographic evidence of hydrogen effects, and replacing the MVC initiation mode observed in an air environment.

In addition, the microscopic appearance of the TTS region could be interpreted as a micro-damage due to hydrogen effects. This experimental fact agrees fairly well wih the descriptions reported by Keefe *et al.* [56], and Nair and Tien [57] about micro-cracking (or micro-damage) produced by the hydrogen.

More evidence of the close relationship between TTS and the hydrogen presence can be found by testing samples in the same chemical solution under different electro-chemical potentials. In these tests, tearing topography surface appears only under cathodic potentials, but not under anodic ones [58], the former associated with hydrogen embrittlement, and the latter with anodic dissolution [1].

Finally, there is another fact which supports the assumption of TTS mode revealing hydrogen effects: the relation between the compressive residual stresses in the vicinity of the crack tip due to fatigue precracking and the extension of the TTS region. It has been proved [59, 60] that TTS depth is a decreasing function of the absolute value of compressive residual stresses in the vicinity of the crack tip. The stronger the fatigue load, the higher the compressive residual stresses, and the less the hydrogen penetrates into the sample.

4.2. Role of hydrostatic stress in hydrogen diffusion

The second key point to discuss is the influence of the hydrostatic stress on diffusion of hydrogen. To study the influence of that variable, elastic–plastic finite element computations were performed with the four geometries used in the experimental programme [34, 55], and the evolution of hydrostatic stress was analysed, in order to compare it with the extension of the TTS zone. The main results are discussed below.

The point of maximum hydrostatic stress (very important in hydrogen diffusion according to Equation 27), is a characteristic geometric datum: it does not depend on the load applied to the sample, but remains constant throughout the loading process. In samples A and C this point is located near the notch tip (surface of the sample). For geometries B and D it is in the centre of the sample. Fig. 6 shows the typical hydrostatic stress distributions in the notched samples, where x_s is the depth of the maximum hydrostatic stress point, measured from the notch surface.

In Fig. 7 the depth of the TTS zone, x_{TTS}, versus the duration of the test (time to rupture of the sample, t_c, exposed in hours) is plotted. A horizontal line corresponding to the value x_s (depth of the maximum hydrostatic stress point) is also represented for each geometry. The depth of the TTS region increases when the duration of the test increases, that is, when the displacement rate falls (there being a longer period for hydrogen to diffuse).

The asymptotic value of x_{TTS} for quasi-instantaneous tests is not zero. This fact demonstrates that the embrittlement effect of hydrogen is not negligible, even for very short durations of the test. It is possible to write:

$$\lim_{t_c \to 0} x_{TTS} = \lim_{\dot{\varepsilon} \to \infty} x_{TTS} = x_0; \quad x_0 = x_0 \text{ (geometry)} \quad (28)$$

where $\dot{\varepsilon}$ represents the strain rate in the test. In this case the boundary condition (Equation 26) for the diffusion differential equation is reached almost instantaneously.

The asymptotic value of x_{TTS} for quasi-static tests coincides with x_s, the depth of the maximum hydrostatic stress point, that is

$$\lim_{t_c \to \infty} x_{TTS} = \lim_{\dot{\varepsilon} \to 0} x_{TTS} = x_s; \quad x_s = x_s \text{ (geometry)} \quad (29)$$

with the same meanings. The hydrogen concentration

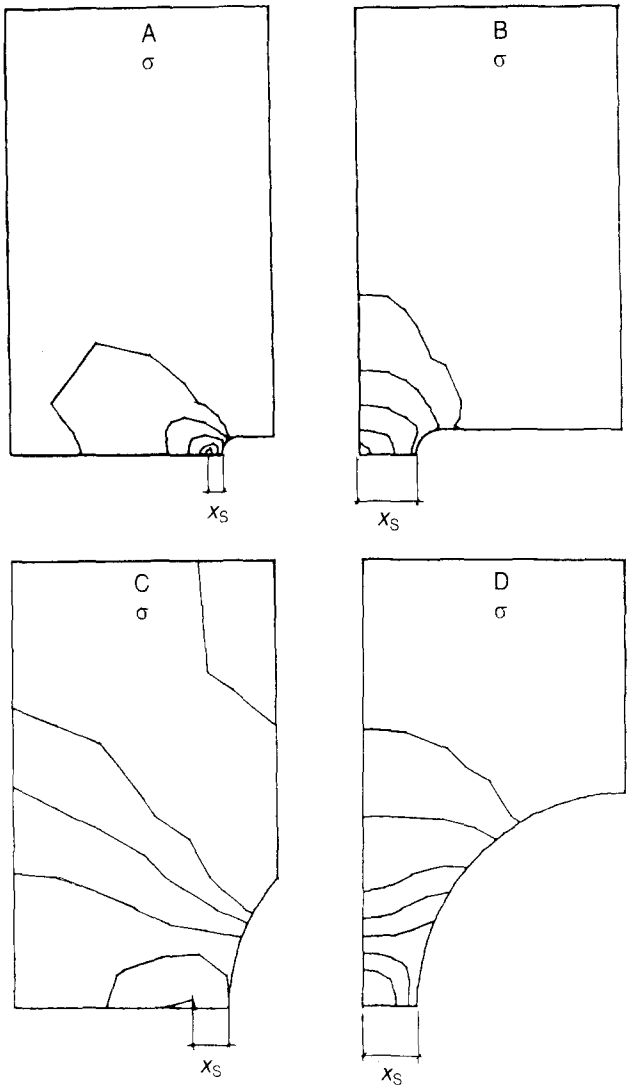

Figure 6 Typical hydrostatic stress distributions in the notched samples: the point at which the hydrostatic stress, σ, reaches a maximum is a characteristic of the geometry. (Results from the elastic-plastic FEM analysis.)

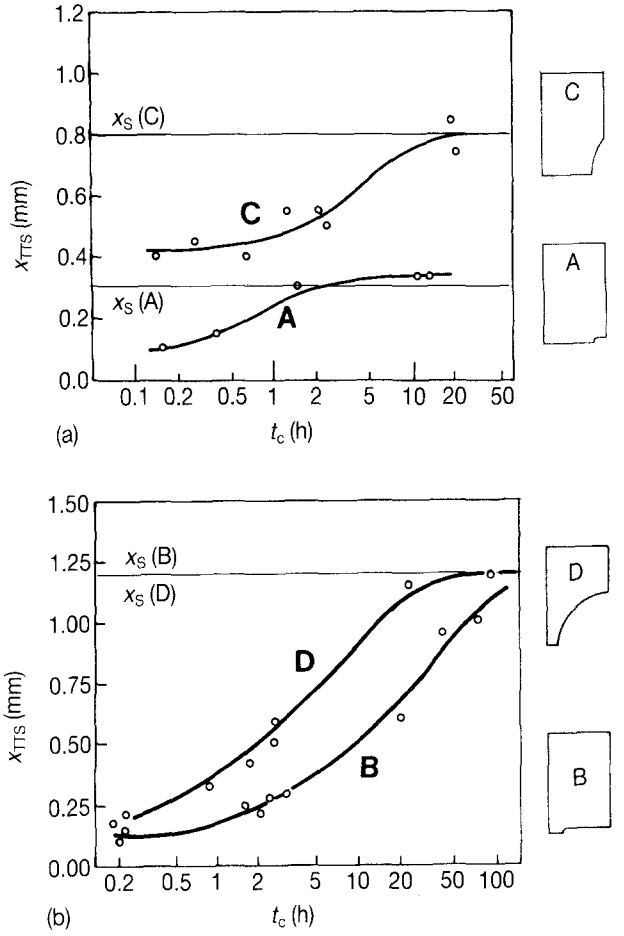

Figure 7 Depth of TTS zone versus time to rupture for all samples; x_s represents the depth of the maximum hydrostatic stress point for each geometry.

in these tests is a direct function of the hydrostatic stress at each point, as stated in Equation 27, because the stationary solution of the diffusion differential equations is an adequate approach in this case.

Regarding the influence on fracture of hydrostatic stress levels, Table IV summarizes the characteristics of each test, the failure load, the TTS size and the boundary and maximum values of the hydrostatic stress at the fracture instant. Values of the factor $\exp(V^*\sigma/RT)$ of Equations 26 and 27 are also represented. From this table, it is possible to assume an appreciable influence of hydrostatic stress on the diffusion of hydrogen, because the values of the multiplication factor lie between 1.26 and 2.77. Because the values of hydrostatic stress change as the load applied on the sample increases in the test, it is very difficult to correlate the triaxial stress levels with the fracture load in a hydrogen environment.

One approach would consist in analysing the role of hydrostatic stress at the boundary sample in the failure load of quasi-instantaneous tests. Because diffusion cannot take place in these tests due to their short duration, the value of σ at the boundary would be relevant, because it influences the hydrogen concentration according to Equation 26. Fig. 8 presents the failure load in a hydrogen environment (divided by the failure load in air) for the quasi instantaneous tests of each geometry, as a function of the boundary hydrostatic stress (in dimensionless exponential form) computed at the fracture instant. There is a direct decreasing relationship between the failure load in the quasi-instantaneous tests and the boundary hydrostatic stress at the fracture instant, which allows a quantification of the influence of such a stress on hydrogen ingress, through the boundary concentration.

Another approach is to study the influence of maximum hydrostatic stress on diffusivity. According to Fig. 7, σ_{max} seems to be relevant in the quasi-static tests. However, this variable does change as the load applied to the sample increases during the test, making difficult a simple numerical approach. It would be useful to consider a parameter related to the maximum hydrostatic stress but remaining constant during the test. In this conceptual frame, the stress triaxiality (ratio of the hydrostatic to the equivalent stress) seems to be adequate, because it is almost constant during the test, as can be seen in Fig. 9, which offers the triaxiality distributions in the notched samples: in elastic regime (a) and plastic regime corresponding to the fracture instant of the air tests (b).

TABLE IV Hydrostatic stress levels in the hydrogen embrittlement tests, computed at the fracture instant

Geometry	$\dot{u}$ ($m\,s^{-1}$)	t_c (s)	F_R/F_0	x_{TTS} (mm)	σ_Γ (MPa)	$\exp\left(\frac{V^*\sigma_\Gamma}{RT}\right)$	σ_{max} (MPa)	$\exp\left(\frac{V^*\sigma_{max}}{RT}\right)$
A	4.79×10^{-7}	555	0.79	0.10	728	1.83	917	2.14
	4.81×10^{-7}	570	0.80	0.10	735	1.84	922	2.15
	1.82×10^{-7}	1365	0.77	0.15	708	1.80	894	2.10
	3.68×10^{-8}	5370	0.70	0.30	667	1.74	817	1.97
	3.96×10^{-9}	39960	0.63	0.34	632	1.69	735	1.84
	3.26×10^{-9}	48600	0.63	0.34	632	1.69	735	1.84
B	1.00×10^{-7}	720	0.86	0.10	603	1.65	1147	2.59
	1.03×10^{-7}	780	0.90	0.15	618	1.67	1228	2.77
	1.02×10^{-8}	5760	0.79	0.25	574	1.61	1004	2.30
	8.70×10^{-9}	7380	0.82	0.21	581	1.62	1067	2.42
	6.90×10^{-9}	8520	0.79	0.27	574	1.61	1004	2.30
	6.23×10^{-9}	11160	0.85	0.30	596	1.64	1118	2.53
	6.02×10^{-10}	75600	0.69	0.60	536	1.56	835	2.00
	1.87×10^{-10}	143040	0.48	0.93	456	1.46	559	1.59
	1.12×10^{-10}	262800	0.52	1.00	464	1.47	603	1.65
C	1.83×10^{-6}	516	0.91	0.40	566	1.60	625	1.68
	9.71×10^{-7}	972	0.91	0.45	566	1.60	625	1.68
	3.45×10^{-7}	2295	0.87	0.40	543	1.57	596	1.64
	1.54×10^{-7}	4500	0.84	0.55	528	1.55	574	1.61
	6.67×10^{-8}	7560	0.77	0.55	489	1.50	528	1.55
	5.47×10^{-8}	8340	0.75	0.50	480	1.49	512	1.53
	5.85×10^{-9}	68400	0.72	0.85	456	1.46	497	1.51
	5.33×10^{-9}	75000	0.72	0.75	456	1.46	497	1.51
D	2.13×10^{-7}	660	0.91	0.10	379	1.37	589	1.63
	2.06×10^{-7}	780	0.95	0.21	397	1.39	611	1.66
	4.55×10^{-8}	3240	0.92	0.33	388	1.38	596	1.64
	2.45×10^{-8}	6300	0.93	0.41	388	1.38	603	1.65
	1.49×10^{-8}	9000	0.90	0.60	379	1.37	581	1.62
	1.35×10^{-8}	9420	0.88	0.50	370	1.36	574	1.61
	6.98×10^{-10}	182400	0.88	1.15	370	1.36	574	1.61
	3.93×10^{-10}	324000	0.88	1.20	370	1.36	574	1.61

$\dot{u}$, displacement rate; x_{TTS} depth of the TTS region; $V^* = 2\,cm^3\,mol^{-1}$ [2]; t_c, time to failure or critical time; σ_Γ, hydrostatic stress at the sample boundary (fracture instant); $T = 290\,K$; F_R/F_0, failure load in solution/failure load in air; σ_{max}, maximum hydrostatic stress in the sample (fracture instant).

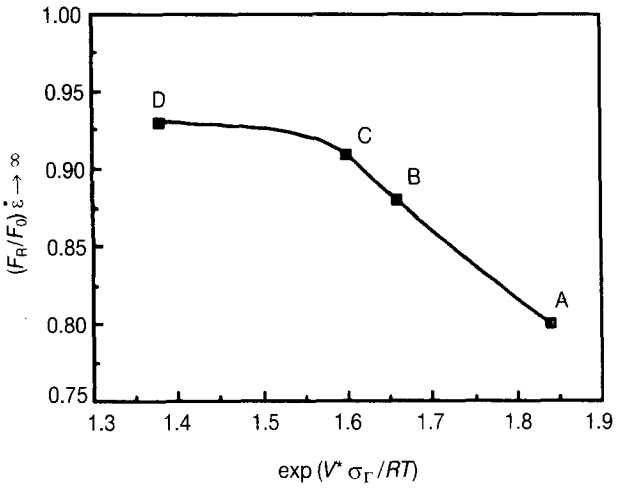

Figure 8 Relationship between the asymptotic value of the failure load in hydrogen environment for quasi-instantaneous tests and the hydrostatic stress at the boundary, computed at the fracture instant.

Results are taken from the elastic–plastic finite element model (FEM) analysis. During the elastic regime the triaxiality does not change. In the plastic regime there is a small change. The SSRT are between both values. A triaxiality factor, T, can be defined as the maximum value of the stress triaxiality in the sample

$$T = \sup_{\Omega}(\sigma/\bar{\sigma}) \tag{30}$$

where σ is the hydrostatic stress, $\bar{\sigma}$ the equivalent stress (in the Von Mises sense) and Ω the domain. The triaxiality factor, T, was computed from the elastic distribution, and the resulting values for geometries A, B, C and D were 0.9, 1.4, 0.5 and 0.4, respectively. Fig. 10 shows the failure load in the quasi-static tests versus the triaxiality factor of each geometry. It is possible to observe a monotonic decreasing dependence, which emphasizes the role of maximum hydrostatic stress in hydrogen diffusion.

5. Conclusions

1. A set of equations describing hydrogen diffusion was formulated, based on thermodynamic principles. The diffusion is stress-assisted, and the hydrogen moves not only to the minimum concentration sites, but also towards the maximum hydrostatic stress locations.

2. The tearing topography surface (TTS), a new microscopic fracture mode, is associated with hydrogen effects, and it seems to consist of micro-damage or micro-tearing produced by the hydrogen.

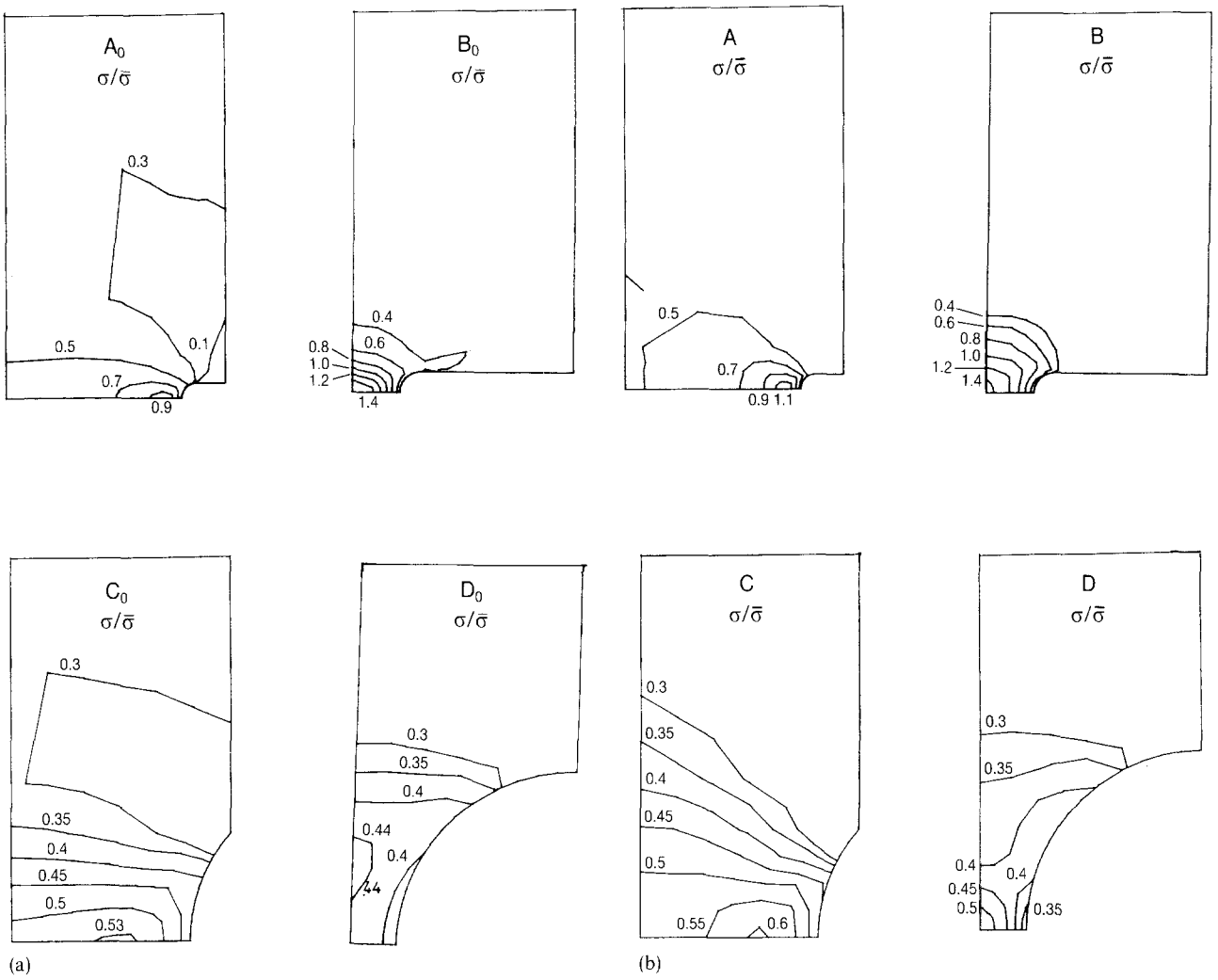

Figure 9 Triaxiality distributions in the notched samples: (a) elastic regime, (b) plastic regime corresponding to the fracture instant of the air tests (results from the elastic-plastic FEM analysis).

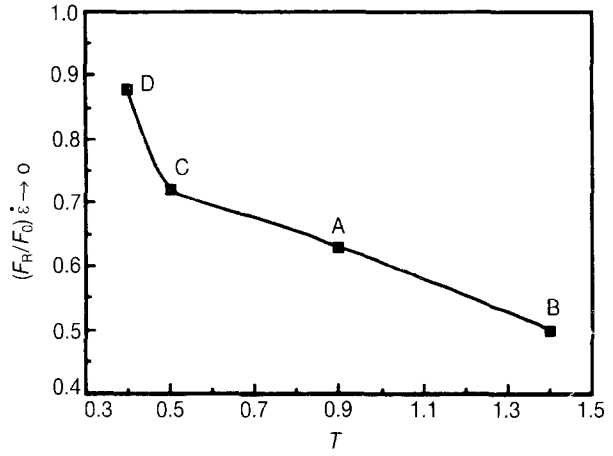

Figure 10 Relationship betwen the asymptotic value of the failure load in hydrogen environment for quasi-static tests and the triaxiality factor (maximum value of the triaxiality in the sample, a characteristic of the geometry).

3. The hydrostatic stress plays a relevant role in accelerating the diffusion of hydrogen in the sample, both increasing the boundary concentration and enhancing the hydrogen flux associated with stress gradients.

4. The hydrostatic stress at the boundary controls the fracture of the sample in the quasi-instantaneous tests, fast enough to avoid hydrogen penetration towards the inner points. In this case the environmental effect is restricted to the notch tip.

5. The triaxiality factor (maximum triaxiality in the sample) governs the fracture of the sample in the quasi-static tests, slow enough to allow the stationary solution of the diffusion problem to be reached. In this case the environmental effect depends on the hydrogen diffusion towards the maximum hydrostatic stress points.

Acknowledgements

This work was supported by the Polytechnical University of Madrid (Spain), under Grant A9000200161. The author thanks Dr A. M. Lancha for performing the scanning electron microscopy, and Mr J. Monar, Nueva Montaña Quijano Company, Santander, Spain, for providing the steel used in the experimental programme. Helpful discussions of this paper by Professor M. Elices and Professor J. Planas, Polytechnical University of Madrid, are also acknowledged.

References

1. R. N. PARKINS, M. ELICES, V. SANCHEZ-GALVEZ and L. CABALLERO, *Corros. Sci.* **22** (1982) 379.
2. J. P. HIRTH, *Metall. Trans.* **11A** (1980) 861.

3. H. H. JOHNSON, J. G. MORLET and A. R. TROIANO, *Trans. Met. Soc. AIME* **212** (1958) 528.
4. A. R. TROIANO, *Trans. ASM* **52** (1960) 54.
5. W. W. GERBERICH, Y. T. CHEN and C. ST. JOHN, *Metall. Trans.* **6A** (1975) 1485.
6. W. W. GERBERICH, T. LIVNE, X. F. CHEN and M. KACZOROWSKI, *ibid.* **19A** (1988) 1319.
7. H. P. VAN LEEUWEN, *Engng Fract. Mech.* **9** (1977) 291.
8. *Idem, ibid.* **6** (1974) 141.
9. M. A. ASTIZ, in "Computational Methods for Non Linear Problems", edited by C. Taylor, D. R. J. Owen and E. Hinton (Pineridge Press, Swansea, 1987) p. 271.
10. C. HWANG and I. M. BERNSTEIN, *Acta Metall.* **34** (1986) 1001.
11. *Idem, ibid.* **34** (1986) 1011.
12. J. K. TIEN, A. W. THOMPSON, I. M. BERNSTEIN and R. J. RICHARDS, *Metall. Trans.* **7A** (1976) 821.
13. H. H. JOHNSON and J. P. HIRTH, *ibid.* **7A** (1976) 1543.
14. S. V. NAIR, R. R. JENSEN and J. K. TIEN, *ibid.* **14A** (1983) 385.
15. A. J. WEST and M. R. LOUTHAN Jr, *ibid.* **10A** (1979) 1675.
16. *Idem, ibid.* **13A** (1982) 2049.
17. T. ZAKROCZYMSKI, *Corrosion* **41** (1985) 485.
18. M. HASHIMOTO and R. M. LATANISION, *Metall. Trans.* **19A** (1988) 2789.
19. J. P. HIRTH and B. CARNAHAN, *Acta Metall.* **26** (1978) 1795.
20. F. R. BROTZEN and A. SEEGER, *ibid.* **37** (1989) 2985.
21. S. OCHIAI, S. YOSHINAGA and Y. KIKUTA, *Trans. ISIJ* **15** (1975) 503.
22. Y. KIKUTA, S. OCHIAI and T. KANGAWA, in "Proceedings of the 2nd International Congress on Hydrogen in Metals", Paris 1977, Paper $3F_1$.
23. R. A. ORIANI, *Acta Metall.* **18** (1970) 147.
24. J. O'M. BOCKRIS and P. K. SUBRAMANYAN, *J. Electrochem. Soc.* **118** (1971) 1114.
25. G. M. PRESSOUYRE and I. M. BERNSTEIN, *Metall. Trans.* **9A** (1978) 1571.
26. G. M. PRESSOUYRE, *ibid.* **10A** (1979) 1571.
27. G. M. PRESSOUYRE and I. M. BERNSTEIN, *Acta Metall.* **27** (1979) 89.
28. G. M. PRESSOUYRE, *ibid.* **28** (1980) 895.
29. G. M. PRESSOUYRE and I. M. BERNSTEIN, *Metall. Trans.* **12A** (1981) 835.
30. M. IINO, *Acta Metall.* **30** (1982) 367.
31. *Idem, ibid.* **30** (1982) 377.
32. *Idem, Metall. Trans.* **16A** (1985) 401.
33. B. G. POUND, *Corrosion* **45** (1989) 18.
34. J. TORIBIO, PhD thesis, Polytechnical University of Madrid (1987).
35. J. TORIBIO and M. ELICES, in "Proceedings of CORROSION/88 – Corrosion Research Symposium", St Louis, MO, March 1988 (NACE, 1988) p. 88.
36. V. SANCHEZ-GALVEZ, L. CABALLERO and M. ELICES, ASTM STP **866**, edited by G. Haynes and R. Baboian (American Society for Testing and Materials, Philadelphia, PA, 1985) p. 428.
37. G. BURNELL, D. HARDIE and R. N. PARKINS, *Br. Corros. J.* **22** (1987) 229.
38. C. D. KIM and B. E. WILDE, ASTM STP **665**, edited by G. M. Ugiansky and J. H. Payer (American Society for Testing and Materials, Philadelphia, PA, 1979) p. 97.
39. B. R. W. HINTON and R. P. M. PROCTER, *Corros. Sci.* **23** (1983) 101.
40. M. HASHIMOTO and R. M. LATANISION, *Metall. Trans.* **19A** (1988) 2799.
41. Y. J. PARK and I. M. BERNSTEIN, in "Proceedings of the 4th International Conference on Fracture – ICF4", Waterloo 1977, edited by D. M. R. Taplin (University of Waterloo Press, Waterloo, 1977) p. 33.
42. *Idem, Metall. Trans.* **10A** (1979) 1653.
43. J. J. LEWANDOWSKI and A. W. THOMPSON, *ibid.* **17A** (1986) 461.
44. *Idem, ibid.* in "Advances in Fracture Research – ICF6", edited by S. R. Valluri, D. M. R. Taplin, P. Rama Rao, J. F. Knott and R. Dubey (Pergamon Press, Oxford, 1984) p. 1515.
45. *Idem, Metall. Trans.* **17A** (1986) 1769.
46. *Idem, Acta Metall.* **35** (1987) 1453.
47. M. DOLLAR, I. M. BERNSTEIN and A. W. THOMPSON, *ibid.* **36** (1988) 311.
48. K. NAKASE and I. M. BERNSTEIN, *Metall. Trans.* **19A** (1988) 2819.
49. D. J. ALEXANDER and I. M. BERNSTEIN, *ibid.* **20A** (1989) 2321.
50. A. FONTAINE and S. JEUNEHOMME, in "Failure Analysis. Theory and Practice – ECF7", edited by E. Czoboly (Engineering Materials Advisory Services Ltd, West Midlands, 1988) p. 1267.
51. A. FONTAINE and S. JEUNEHOMME, in "Advances in Fracture Research – ICF7", edited by K. Salama, K. Ravi-Chandar, D. M. R. Taplin and P. Rama Rao (Pergamon Press, Oxford, 1989) p. 3865.
52. J. J. LEWANDOWSKI and A. W. THOMPSON, in "Fracture Control of Engineering Structures – ECF6", edited by H. C. van Elst and A. Bakker (Engineering Materials Advisory Services Ltd, West Midlands, 1986) p. 1985.
53. A. W. THOMPSON and J. C. CHESNUTT, *Metall. Trans.* **10A** (1979) 1193.
54. J. E. COSTA and A. W. THOMPSON, *ibid.* **13A** (1982) 1315.
55. J. TORIBIO, A. M. LANCHA and M. ELICES, *Mater. Sci. Engng*, **A145** (1991) 167.
56. P. W. KEEFE, S. V. NAIR and J. K. TIEN, *Metall. Trans* **15A** (1984) 1865.
57. S. V. NAIR and J. K. TIEN, *ibid.* **16A** (1985) 2333.
58. A. M. LANCHA, PhD thesis, Complutense University of Madrid (1987).
59. A. M. LANCHA and M. ELICES, in "Proceedings of corrosion/88 – Corrosion Research Symposium", St Louis, MO, March 1988 (NACE, 1988) p. 95.
60. *Idem*, in "Failure Analysis. Theory and Practice – ECF7", edited by E. Czoboly (Engineering Materials Advisory Services Ltd, West Midlands, 1988) p. 961.

Received 2 October 1991
and accepted 11 August 1992